# VCU

Virginia Commonwealth University

## VCU Scholars Compass

2020

# A Density Functional Theory Study of Palladium Nanoparticles and Their Redox Properties on Graphene

Billie A. Radcliffe

# A Density Functional Theory Study of Palladium Nanoparticles and Their Redox Properties on Graphene

A thesis submitted in partial fulfillment of the requirements for

the degree of Master of Science at Virginia Commonwealth University.

By

Billie Ann Radcliffe

Bachelor of Science in Physics, Virginia Commonwealth University, 2015

Advisor: Dr. Shiv N. Khanna

Virginia Commonwealth University

Richmond, Virginia

July 2020

# Acknowledgments

First and foremost, I would like to thank Dr. Shiv Khanna and Dr. Arthur Reber for their support and leadership during my time in the VCU physics department. They have been incredibly encouraging mentors and have always lead me down a path of success. I would especially like to thank Dr. Reber for answering what seemed like an endless list of questions, and for his patience when teaching me topics that I felt I would never grasp. I would like to express my deepest and sincerest thanks to my family and friends for being supportive of my ever-changing career goals and aspirations. Additionally, I would especially like to thank my fiancé Cory, for pushing me to always reach for the stars, and my success would not have been possible without his late-night pep talks and constant drive. I am especially grateful for the guidance and advice given to me by Dr. Frank Gupton and the whole Gupton family. Throughout my time at Virginia Commonwealth University, the Gupton family has been a constant reminder of how precious the relationships you can build by chance really are. A big thank you to Thomas, Sam, and Annie for keeping me young and being a perfect escape from science when I needed it. I also wish to thank Dr. Massimo Bertino and Loren Picco for being amazing teachers as well as role models during my time at VCU Physics. Thank you to the whole Gupton Catalysis Group who were ever supportive of their odd physicist colleague. Last but certainly not least, thank you to my furry companions who would sleep on my feet through the wee hours of the morning as I typed this labor of love. Your purrs and woofs were greatly appreciated.

Table of Contents

# List of Figures & Tables

# Abstract

## A DENSITY FUNCTIONAL THEORY STUDY OF PALLADIUM NANOPARTICLES ON GRAPHENE AND RELATED WORK

Nanoparticles exhibit characteristics that are different from bulk materials as well as from atoms resulting in their application in numerous fields of applied material science. In particular, small palladium nanoparticles supported on graphene have been found to be outstanding catalysts for the Suzuki cross-coupling reaction. One explanation as to why these supported nanoparticles are such outstanding catalysts is because they may act as both electron donors and acceptors. Charge donating ligands are known to lower the ionization energy of clusters, making the clusters better donors. In this project, it is hypothesized that graphene supports may also act like charge donating ligands, lowering the ionization energy and making the supported catalyst a better charge donor. To understand his hypothesis we investigate the structure, and energetics of small Palladium (Pd) clusters of 1-7 and 13 atoms as free clusters, and on different graphene-based supports using gradient-corrected density functional theory. Graphene is found to increases the stability of the supported clusters and we find that graphene also significantly reduces the ionization energy of the palladium clusters, which is consistent with the hypothesis that graphene is a good support for catalytic processes in part because it makes the cluster a better charge donor.

By Billie Ann Radcliffe, M.S.

A thesis submitted in partial fulfillment of the requirements for the degree of Master of Science at Virginia Commonwealth University.

Virginia Commonwealth University, 2020.

Advisor: Dr. Shiv N. Khanna

# Chapter 1. Background & Motivation

## 1.1 Objective

The understanding of the behavior of particles at the nanometer scale has proved to be an important advancement in many fields of material sciences, and especially catalysis[1,2]. Many particles, specifically metals display unique chemical and physical characteristics as they move away from bulk crystalline phases and into the nanometer scale. This size dependence can be quite extreme at the subnanometer scale, where every atom counts, and the addition or the removal of a single atom change significantly change a particles' properties.[3–9] This unique behavior can be especially useful for fields where metals and metal-oxides are placed upon a surface support, where the unique properties of the nanoparticles can be stabilized and used for catalysis.[10–13] At these sizes chemical properties are extremely sensitive to changes in both the environment and morphology of the particles adhered on the surface[6,10,14–16].
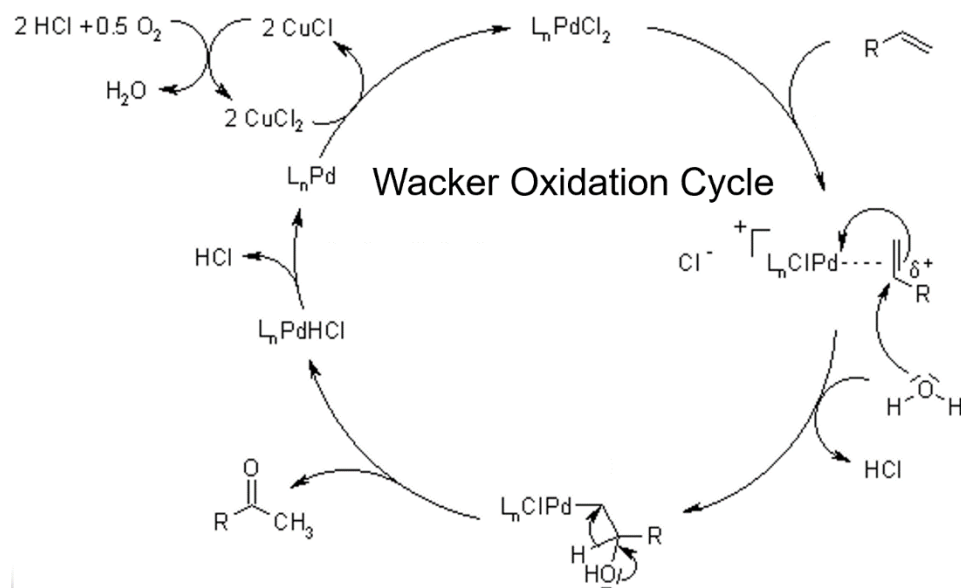


Figure 1. Wacker catalytic process[17], an early example of palladium catalysts in use.

Palladium (Pd) nanoparticles are used in multiple well-defined catalytic processes[18]. For example, Wacker oxidation[19], as well as Buckwald-Hartwig coupling [20] shown in Fig. 1, and Suzuki reactions[18] generally rely on Pd particles Each of these reactions can be optimized by fine

tuning the particles parameters for a specific reaction. One challenge in understanding the activity of nanoparticles for catalysis is their redox properties. For a single palladium atom, the palladium will have a well-defined oxidation state, and by cycling through different oxidation states, the palladium atom may act as an electron donor, or an electron acceptor. In the case of a nanoparticle, once the particle has lost an electron, the electron-hole is delocalized over the particle, so the oxidation state is not well-defined. For this reason, the redox properties of supported clusters are of great interest in order to understand how the support effects the catalysts' ability to donate or accept charge.

For the Suzuki cross-coupling reactions, palladium supported on microwaved graphene has been shown to be an outstanding heterogeneous catalyst.[10,11,16,20–22] Our hypothesis for the high activity of palladium supported on graphene is that the graphene serves as a reservoir of charge that allows the cluster to act as a superior charge donor. The initial oxidative addition step for a Suzuki reaction requires that the cluster donate charge to the reactants. Previous research in the Khanna and Gupton groups found that the graphene dramatically lowered the activation energy for this reaction, and that this was driven by the enhanced charge donating ability of the clusters supported on graphene. The graphene also allowed the supported cluster to act as an effective charge acceptor, revealing that the metallic behavior of the graphene played a critical role in the activity of the supported clusters.[10,16] For this reason, a quantitative theoretical study was performedon the effect of the graphene support on the redox properties of the supported palladium clusters.

In order to better understand the redox properties of palladium clusters supported on graphene supports, we investigated the characteristics of Palladium (Pd) particles ranging in size from a single atom, to an atomic cluster of 13 atoms $Pd_n$, n=1-7,13. We investigated free palladium clusters, as well as clusters supported on various defects associated with a graphene model surface. In particular, we are interested in the ionization energy of these clusters and would like to know the effect of the support on the ionization energy. It is known that by attaching charge donating ligands to Pd allows the clusters to become a better charge donors.[23–28] Our hypothesis is that graphene based supports can act much like a charge donating ligand and that it will reduce the ionization energy of the supported palladium cluster, confirming that the support makes the cluster a better charge donor and eases the change in charge states as needed for catalytic

applications. .[22,27,29,30] In addition, the binding energies of the Pd clusters $n = 1 - 7, 13$ were caluated using DFT at neutral charge as well as in the +1, and +2 state. Based upon previous work, the ionization energies were computed for clusters in those sizes. Pristine graphene and single and double vacancy graphene were chosen to study this relationship. By placing optimized Pd clusters onto a graphene support and calculating the ground-state energies of these clusters, binding energies, and ionization energies, we hoped to gain knowledge about the support's role on the redox properties of Pd supported particles.

## 1.2 Computational Approach

Ground state structures of the Pd clusters were obtained using the Amsterdam Density Functional (ADF) simulation packages. The ADF[31] program is unique because it uses basis sets that are built from Slater-type orbital (STO) functions. These functions are given by,

$$\Upsilon_{lm}(\Omega)r^n e^{-\alpha r} = f(r) \qquad\qquad 1$$

where $\Upsilon_{lm}$, is a spherical harmonic with a decay factor of $\alpha$. This decay factor greatly improves the number of basis sets needed to reach chemical accuracy. Additionally, the ADF package has capabilities of calculating ground state energies using a symmetrical approach or one without a symmetry restriction[31]. This was crucial in our understanding of the cluster sizes we investigated because it allowed us to manually manipulate the spacing between atoms which was of note for clusters in the tetrahedral and pyramidal geometry.

ADF also utilizes a frozen core, which treats the deeper atomic orbitals as fixed, which cuts down on computational time and increase accuracy. When molecules, or for our case, clusters, change bonding states, the center orbitals change very little and do not contribute to bond formation as much as the outer orbitals, therefore it is sound reasoning to leave them out of the calculation. The Zero-Order Regular Approximation (ZORA)[32] is used to account for the scalar-relativistic effect, which ignores spin-orbit interactions. The self-consistent field (SCF)[31] procedure is used to solve the Kohn-Sham equations as expressed in the previous chapter and ADF employs direct inversion if iterative subspace (DIIS) to obtain convergence of the SCF to reach results.

# Chapter II Introduction

## 2.1 Density Functional Theory

Developments in quantum mechanical sciences have allowed researchers to predict the behavior of atomic clusters and other solid-state materials, which are useful for various applications[33]. Catalysis, technology, and energy storage all rely on the optimal performance of such materials, and thus, by gaining knowledge about certain classes, we can make advancements in developing novel substances, which help to make these processes more efficient and/or cost effective[1,33]. Since the early 1900s, quantum mechanical theory has been making great strides towards a complete understanding in material science behavior, and the development of Density Functional Theory has revolutionized the ease at which we can calculate many ground-state properties such as binding energy, band diagrams, and molecular orbitals[34].

Starting with the discovery of the de Broglie wavelength and the Heisenberg's Uncertainty Principle, the foundations of quantum mechanics were born. We understand from Heisenberg that the act of measurement blocks us from describing the exact position and momentum of a particle within a system. Thus, the tactic of making approximations and simplifications in a system becomes a large part of the mathematical development that leads to the eventual discovery of modern-day molecular dynamics. Based on the theory of particle-wave duality, all a system's characteristics can be defined by the solution of its wave function, $\Psi$[35]. Edward Schrödinger defined this wavefunction as,

$$\hat{H}\Psi = E\Psi \qquad\qquad 2$$

where $\hat{H}$ is defined as the Hamiltonian Operator, the sum of the system's kinetic and potential energies[35,36]. When expanded, the Schrödinger Equation becomes,

$$-\frac{\hbar}{2m}\nabla^2\Psi(r) + V(r)\,\Psi(r) = E\Psi(r) \qquad\qquad 3$$

This equation (2) describes any system as a sum of its constituent energetic parts. The simplest explanation of this equation can be described using the Hydrogen atom, or Hydrogen-like systems, as an example.

The mass term in equation (2) represents the total mass of the system, and so we must define this further in the case of the Hydrogen atom to be the mass at the center of gravity. This becomes,

$$m = \frac{mM}{m+M} = \mu \qquad\qquad 4$$

where, $M$ is the mass of the nucleus and $m$ is the mass of the electron.

Additionally, we must define the potential energy term. This can be comprehensively expressed by a Coulombic term as,

$$5$$
$$V(r) = -\frac{Ze^2}{4\pi\epsilon_0 r}$$

where $Ze$ is the charge of the nucleus, $e$ is the charge of the electron, and $\epsilon_0$ is the permittivity of vacuum. Expanding the original equation (2) for the above points we have,

$$-\frac{\hbar}{2\mu}\nabla^2 - \frac{Ze^2}{4\pi\epsilon_0 r} = E\Psi(r) \qquad\qquad 6$$

which is the full representation of the Schrödinger equation for the Hydrogen atom. When (5) is further expanded into polar coordinates,

$$-\frac{\hbar}{2\mu}\left[\frac{1}{r^2}\frac{\partial}{\partial r}\left(r^2\frac{\partial\psi}{\partial r}\right) + \frac{1}{r^2 \sin\theta}\frac{\partial}{\partial\theta}\left(\sin\theta\frac{\partial\psi}{\partial\theta}\right) + \frac{1}{r^2\sin^2\theta}\frac{\partial^2\psi}{\partial\phi^2}\right] - \frac{Ze^2}{4\pi\epsilon_0 r}\Psi = E\Psi \qquad 7$$

it can be solved using separation of variables to receive a solution such as,

$$\psi(r,\theta,\phi) = R(r)\Theta(\theta)\Phi(\phi) = NR_{n.l}(r)P_l^m(\cos\theta)e^{im\phi} \qquad\qquad 8$$

which has defined 3 quantum numbers, *n, l,* and *m.* These numbers define the probability density of the system which they are derived[37] of therefore, if we can find a solution to the Schrödinger equation for any given system, we will have a great deal of understanding regarding its ground-state characteristics. This leads to an understanding of what the molecular orbitals will look like, as well as a picture of how the system will create chemical bonds, excited states, and so on.

However, there exists a many-body problem.

In practice, a discrete solution to the Schrödinger Equation becomes increasingly difficult as you add more degrees of freedom, i.e. particles, into a system therefore we must make some approximation in order to make calculation easier. The Born-Oppenheimer Approximation states that the motion of the nucleus can be treated as fixed[35] due to its mass being many orders of magnitude larger than the electron cloud within the system. The solution to the system's wavefunction depends on the position of the nucleus in relation to the electrons, but not on the motion of the nucleus itself. The Schrodinger equation can now be written as,

$$[\sum_{i=1}^{N} -\frac{1}{2}\nabla^2 + \sum_{j=1}^{M} V_{ex}(r_i) + \sum_{i=1}^{N}\sum_{j<1}^{M} V_{ee}(r_i, r_j)]\Psi = E\Psi \tag{9}$$

where the first term represents the kinetic energy, the second term the external potential applied from the nucleus, and the third term is the electron-electron interactions within the system.

The solutions to equation (8) begin the development of modern-day Density Functional Theory starting with the Hohenburg-Kohn theorem.

## 2.2 Hohenburg – Kohn

This theorem has two distinct parts. The first states that the external potential $(V_{ex})$ and the total energy $E$ is a unique function of the electron density[38], $(\rho_{\vec{r}})$. This is expressed as,

$$E(\rho(\vec{r})) = \int \rho(\vec{r})V_{ext}(\vec{r})d\vec{r} + F(\rho(\vec{r})) \tag{10}$$

where $F(\rho(\vec{r}))$ is a function of the electron density. This can also be expressed in terms of the Hamiltonian similar to the Schrodinger Equation as,

$$E(\rho(\vec{r})) = \ <\Psi\hat{H}\Psi> \tag{11}$$

and expanding this it becomes,

$$E(\rho(\vec{r})) = T(\rho) + V_{ee}(\rho) + \int \rho(\vec{r})V_{ext}(\vec{r})d\vec{r} \tag{12}$$

Equation (11) points to the second part of the Hohenburg-Kohn Theorem, the density that minimizes the total energy is the exact ground-state energy. This states that if a certain density $\rho(\vec{r})$ satisfies the conditions,

$$N = \int \rho(\vec{r})d\vec{r} \qquad\qquad 13$$

and

$$\rho(\vec{r})d\vec{r} \leq 0 \qquad\qquad 14$$

then the energy of the system should be satisfied by,

$$E_o \leq E_V(\rho) \qquad\qquad 15$$

where $E_V(\rho)$ is a functional of equation (11). These two theorems together make up the bulk of Density Functional Theory and allow for the solution to the Schrodinger equation to be calculated.

## 2.3 Kohn-Sham

While Hohenburg-Kohn (*H.K.*) set up the solution to the ground state electron density, Kohn-Sham Theory helps us facilitate that calculation by creating a system that is non-interacting, reducing the degrees of freedom in the calculation[38]. Let us return to the *H.K.* Hamiltonian expression in equation (10). In early quantum theory, the kinetic energy of a many body system could not be calculated discretely, so where H.K. theorem creates a self-satisfying variational problem with the electron energy conserved, this leads to,

$$\delta[F(\rho(\vec{r}))] + \int \rho(\vec{r})V_{ext}(\vec{r})d\vec{r} - \mu(\int n(\vec{r})d\vec{r} - N)] = 0 \qquad\qquad 16$$

where the new term $\mu$ is a Lagrange multiplier in reference to the conserved electrons $N$. This is given by,

$$\mu = \frac{\delta F(\rho(\vec{r}))}{\delta\rho(\vec{r})} + V_{ex}(\vec{r}) \qquad\qquad 17$$

We can now define a new ground-state wavefunction $\Psi_{KS}$ for this non-interacting system. In this wave function the function of the electron density, $F(\rho(\vec{r}))$, can be expanded to contain three distinct energetic terms accounting for the kinetic energy of a Homogeneous Electron Gas (HEG), the Hartree electrostatic energy of electrons, and a new term defined as the Exchange Correlation Energy (XC).

$$[F(\rho(\vec{r}))] = K_{HEG}(\rho(\vec{r})) + E_H(\rho(\vec{r})) + E_{XC}(\rho(\vec{r})) \qquad\qquad 18$$

This term, $E_{XC}(\rho(\vec{r}))$, accounts for the different between non-interacted kinetic energy and the nuclear contribution of those electron-electron interactions within the system. This gives way to,

$$\mu = \frac{\delta K_{HEG}(\rho(\vec{r}))}{\delta\rho(\vec{r})} + V_{KS}(\vec{r}) \tag{19}$$

where $V_{KS}(\vec{r})$ is the Kohn-Sham potential. This can be further expanded in terms of the extract potential by,

$$V_{KS}(\vec{r}) = V_{ex}(\vec{r}) + V_H(\vec{r}) + V_{XC}(\vec{r}) \tag{20}$$

and,

$$V_{XC}(\vec{r}) = \frac{\delta E_{XC}(\rho(\vec{r}))}{\delta\rho(\vec{r})}. \tag{21}$$

This gives a way of solving for the exact ground-state density which can then be calculated by solving the Schrodinger Equation for a system of $N$ electrons. Putting equation (2) in terms of the K.S. potential,

$$[-\frac{1}{2}\nabla^2\Psi(\vec{r}) + V_{KS}(\vec{r})]\,\psi(\vec{r}) = \epsilon_i\psi_i(\vec{r}) \tag{22}$$

where $\epsilon_i$ is a Lagrange multiplier of $N$ and $\psi_i(\vec{r})$ corresponds to the single particle electron orbital. The density can be related to a sum of the $N$ orbitals as,

$$\rho(\vec{r}) = \sum_{i=1}^{N} \psi_i(\vec{r})^2 \tag{23}$$

To have a complete understanding of this relation it is necessary to expand the kinetic energy of the HEG as,

$$K_{HEG}(\vec{r}) = -\frac{1}{2}\sum_{i=1}^{N} \psi_i * (\vec{r})\nabla^2\psi_i(\vec{r})dr \tag{24}$$

Defining the last Kohn-Sham equation for the XC Energy we have,

$$E_{XC}(\vec{r}) = K(\rho(\vec{r})) + K_{HEG}(\rho(\vec{r})) + E_{ee}(\rho(\vec{r})) - E_H(\rho(\vec{r})). \tag{25}$$

The main advantage of the Kohn-Sham approach is that it creates an expression which minimizes the unknown non-interacting energy through the Exchange Correlation energy. Equations (24), (23), and (20) make up the mathematical self-consistent solutions for the ground-state energy and potential.

## 2.4   Applications

Computational methods have emerged as one of the most versatile options for computing various chemical properties of bulk solids, nanoparticles, as well as other types of materials[33,34]. Density functional theory has become by far the most popular method for electronic structure calculations due to the ability to calculate many-electron systems with reasonable accuracy. Its success is largely due to its simplicity and ease of formulation for a wide array of systems as well as the numerous interfacing options for the end user. Put simply, you do not have to be an expert in quantum mechanics to obtain sensible result
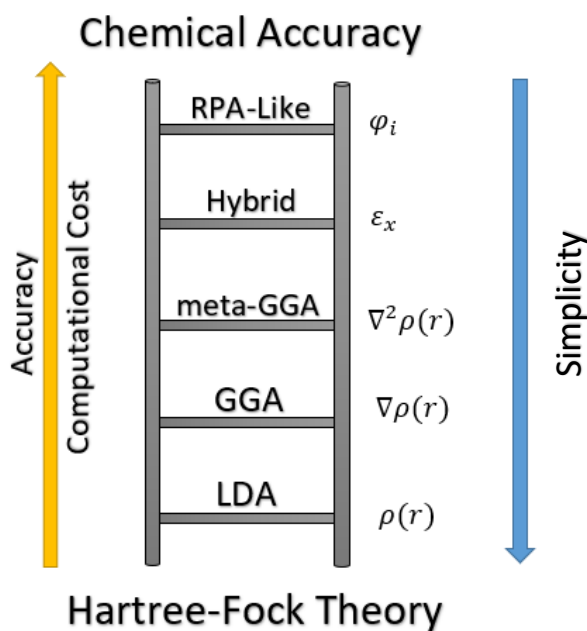


Figure 2. Jacob's Ladder of DFT.

The applications of Density Functional Theory are wide and those in the fields of organic chemistry, physical chemistry, physics and beyond can find a scheme useful for their respective

research. The field of DFT studies has changed over the years and the functionals keep getting better, but that does not come without some cost – both literally and figuratively. Figure 1. shows a favorite version of Jacob's Ladder for DFT. As we climb the ladder toward more chemically accurate packages ("heaven"), we lose some of the reliability of our calculations based on the increasing number of approximations being taken. For example, the first rung of the ladder is local density approximation (LDA) which was the leading method for solids in the early 1980's[39]. This functional within density functional theory finds the exchange-correlation energy as a function of the charge density. Due to its simplicity, and low status on the ladder, while it was easy and quick, it's results often did not match accurately with experimental data[40].

After LDA came generalized gradient approximations (GGA) which increased the accuracy of many calculations especially for chemical systems[41]. GGA functionals find the exchange-correlation energy using both the charge density and the derivative of the charge density. This method was further enhanced to the second derivative of the charge density which is known with inputs from the kinetic energy term as *meta*-GGA[34]. Further, hybrid-DFT was developed in which exchange correlation functionals and Hartree-Fock methods were combined to provide an even more accurate method for calculating ground state densities for solids, clusters, surfaces, and other classes of materials not suitable for the earlier approximations. However, not even this approximation could accurately calculate ground state properties of certain materials such as highly localized systems such as transition metal oxides and struggled to find the correct band-gap energies of semiconductors. This is due to delocalization error and the difficulty in accurately calculating the energy of virtual states in complex materials.

DFT is not without its limitations[42]. Current approximations are still too complex to accurately calculate electronic or quantum characteristics of fluids, due to inaccuracies in Van der Waals interactions[40]. Delocalization error is a significant source of error that lowers accuracy in transition metal oxides, and in processes such as bond disassociation. Also, as systems get larger, DFT tends to provide results which take a long time to compute and are not always reliable based on the ever-present issue self-interacting particles. Density Functional theory is still a widely used approach to investigating novel systems and materials and most likely will stick around as well develop new methods to increase accuracy and as technology allows us to compute these results faster and more accurately.

# Chapter III. Palladium Cluster Properties

## 3.1 Palladium Clusters n=1-7,13

In the present work, palladium clusters were examined with a systematic approach for ground-state binding energies and geometric arrangements. The foundation of this work sets up the background knowledge necessary to understand how these clusters interact with the graphene support.

Figure 3. shows the most stable geometric arrangements of the $Pd_n$ cluster sizes of neutral charge and their binding energy per atom. As is expected, binding energy per atom increases with increasing cluster size. The large jump in B.E. of 0.405eV between $Pd_3$ and $Pd_4$ can be accounted for based on the change from a 2-dimensional arrangement to a 3-dimensional arrangement.
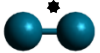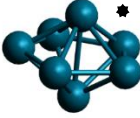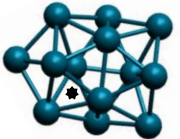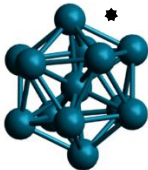
| Ground-state Palladium Clusters | | | |
|---|---|---|---|
| Cluster Size | Structure | Binding Energy (eV) | Spin State |
| 2 | 2.675 Å | 0.543 | 2 |
| 3 | 2.675 Å | 1.097 | 2 |
| 4 | 2.611 Å | 1.502 | 2 |
| 5 | 2.677 Å | 1.615 | 2 |
| 6 | 2.539 Å | 1.747 | 2 |
| 7 | 2.543 Å | 1.877 | 2 |
| 13-o | 2.691 Å | 2.087 | 6 |
| 13-ico | 2.508 Å | 2.079 | 6 |

Figure 3. Ground-state Palladium Cluster Geometry and Binding Energy.

The $Pd_{13}$ cluster is unique in that is has two separate ground-state geometrical arrangements which are both very close in both binding energy and shortest bond length. Due to this we investigate both of these clusters and treat them as two separate particles, $Pd_{13.\ ico}$ & $Pd_{13.\ o}$ as seen in Figure 4.
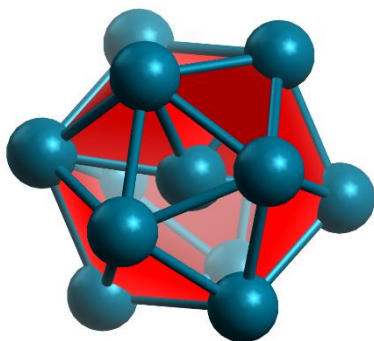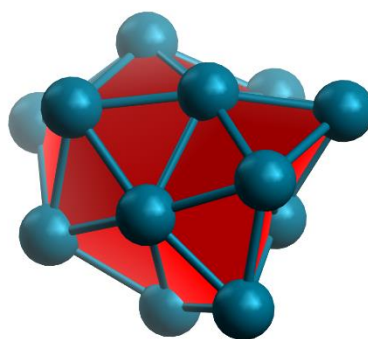


$$Pd_{13,ico} \qquad Pd_{13,o}$$

Figure 4. Geometry of both ground state structure of $Pd_{13}$.

Clusters were given a charge state of +1, and +2 as is seen in previous literature for Pd species[43]. The results found in table 1 were interesting because in the +1-state binding energy tends to be significantly less per atom than in the ground state. This can be explained due to the electronic configuration of the Pd atom – $Kr[4d^{10}]$. Since the valence shell of Palladium is completely occupied, removing one electron is not a very energetically favorable process and so the binding energies of the atoms within the cluster decrease due to this forced instability[44,45].

| Binding Energies for Ionized Clusters | | | | |
|---|---|---|---|---|
| N | Cluster | GS Coh. E./at | +1 B.E./atom | +1 D (Å) | +2 B.E/atom |
| 2 | Pd2 | 0.543 | 1.208 | 2.656 | 5.433 |
| 3 | Pd3 | 1.097 | 0.705 | 2.508 | 0.169 |
| 4 | Pd4 | 1.502 | 0.910 | 2.601 | 0.959 |
| 5 | Pd5 | 1.615 | 0.444 | 2.664 | 0.645 |
| 6 | Pd6 | 1.747 | 0.441 | 2.683 | 0.582 |
| 7 | Pd7 | 1.877 | 0.389 | 2.630 | 0.431 |
| 13 | Pd13 | 2.079 | 1.079 | 6.650 | 1.173 |

Table 1. Energy levels and bond length for clusters at the +1 and +2 state.

As Table 1. shows there is a significant B.E. increase at both the Pd4 and Pd13 cluster size for both the +1 and +2 state. This can be attributed to Jahn-Teller Distortions[44,46] occurring at that size. Due to the molecular arrangement of Pd4 as pyramidal and Pd13 as icosahedral, they are effected by the electronic configuration with $d^9$ arrangement[46].

## 3.2 Palladium Clusters Ionization Energy

It is worth noting that the first ionization energy of the Palladium atom is well defined experimentally and theoretically. From the literature we know that this value is 8.337 eV[44]. Our system using ADF as well as Vienna ab initio Simulation Package (VASP) gives us a I.E. of 8.973 eV, slightly higher. The error present in the calculated value may be due to the parameters set within the simulated system and it is not so egregious such that we should abandon the data.

As the cluster sizes increase as seen in Table 1. the ionization energy decreases. Geometrically our clusters begin to become more tightly packed with increasing cluster side as shown by fluctuating bond length. As these clusters grow, the energy required to remove one electron decreases because the clusters grow outward from the center point in the geometry where the orbitals are the most concentrated and thus the forces are the strongest. These characteristics are most often discussed when reviewing atoms or ionic solids, but metallic clusters also have been seen to express similar behavior[47].

| Ionization Energies of Pd Clusters | | | |
|---|---|---|---|
| n | Cluster | +1 I.E. (eV) | +2 I.E. (eV) |
| 1 | Pd atom | 8.973 | 20.462 |
| 2 | Pd2 | 7.642 | 12.012 |
| 3 | Pd3 | 7.734 | 13.618 |
| 4 | Pd4 | 6.810 | 13.420 |
| 5 | Pd5 | 6.654 | 12.415 |
| 6 | Pd6 | 6.419 | 11.564 |
| 7 | Pd7 | 6.358 | 11.265 |
| 13 | Pd13 | 6.326 | 10.044 |

Table 2. Ionization Energies for Clusters

As with the first ionization energy, our calculated value is very close to the value found in literature through experimental work. Our value for the Pd atom was 20.462 eV where the accepted second I.E. value is typically 19.433 eV. This is a difference of around 1eV similar to the error seen in the +1 state. Additionally, the trend for the second ionization energy is the same as in the first where the energy decreases with increasing cluster size.

## 3.3 Conclusions

The overall  trends in cluster geometry formation are similar to those found in previous studies, and offers a starting point for the structures found on support.[46,48] The ionization energy of the clusters are found to decrease with increasing size. Pd4 is found to be more stable than surrounding sizes, suggesting that it may be a "magic" cluster. In the field of catalysis many conventional palladium particles are grown at the nanometer scale and above. Much research has been completed on the nucleation and growth behaviors of palladium particles[49] and such studies point to scheme of growth following with the Magic-Number theory[46]. In our methodology if we understand the behavior and electronic properties of small clusters, we can use these as a guide

to how larger clusters will interact with the environment. This can lead to predictions regarding catalyst behavior in a reaction mechanism and beyond.

# Chapter 4. Palladium Clusters on Graphene

## 4.1 Graphene Model background

A single plane of carbon atoms bonded in a complete symmetrical hexagonal lattice – graphene. This simple yet elegant substance was once thought to be the greatest development for material science, energy storage, and even physical chemistry and its discovery paved the way for carbon nanotubes, fullerenes and many more carbon allotropes[16,50]. It's excellent status as both a conductor of electricity[16], and heat coupled with its high surface area to mass ratio only increase its allure to scientists[2]. These are some of the reasons graphene and graphene oxide (G.O.) have been used more frequently as supports for various chemical reactions and is the reason we chose it as the theoretical support for our study.

On the scale of our clusters, one cluster placed on a sheet of graphene would seem to create an infinite sea of carbon atoms spread in all directions in relation to the bonding site. This posed a challenge with our calculations in that we had to be extremely diligent to find a graphene sheet size that would give us similar results to those constructed from periodic boundary conditions, but would also be small enough to converge calculations in a reasonable amount of time.
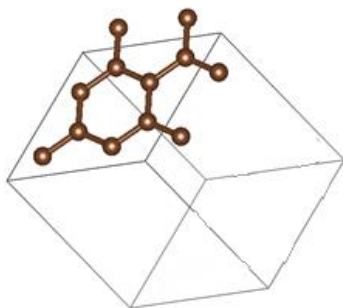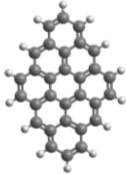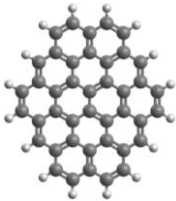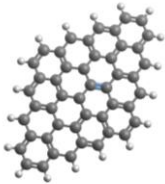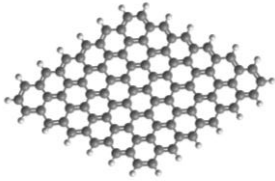


Figure 5. Graphene Unit Cell

As seen in Figure 5. the unit cell of a graphene sheet can be reproduced as many, or as little times as needed for a DFT calculation using cartesian space. Our methodology was to find the

binding energy of an infinite sheet of graphene calculated using VASP and compare that to various sheet sizes calculated using ADF.

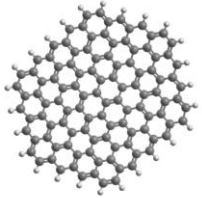| Graphene Sheet Size Optimization | | | |
|---|---|---|---|
| C - C binding Energy from VASP: C98, 8.032 eV | | | |
| **Graphene Sheet Size** | **Carbon Binding Energy (eV)** | **HOMO/LUMO Gap (eV)** | **Support Images** |
| C30 | 9.047 | 1.33 | |
| C42 | 9.317 | 1.63 | |
| C48 | 9.191 | 0.64 | |
| C96 | 8.637 | 0.13 | |

| | | | |
|---|---|---|---|
| C112 | 8.570 | 0.91 |  |

Table 3: Graphene Model Support Sizes and Binding Energy.

As seen in Table 3. the ADF values for the graphene sheet vary with sheet size. While the largest sheet C112 does not exactly match the value calculated from VASP, it was the closest value that also would allow for the smallest computational time. The bond angles of all graphene sheets were also investigated and no significant change in bond lengths or angles was found to change with changing sheet size[51]. On the discrete sheet sizes with terminating hydrogens around the edges, as seen in Figure 6. The sheet was seen to decompose from the original 2-D expected plane. This is due to there being less electric effects on the edges of the sheet and was not seen to cause issues with both convergence or binding energy values.



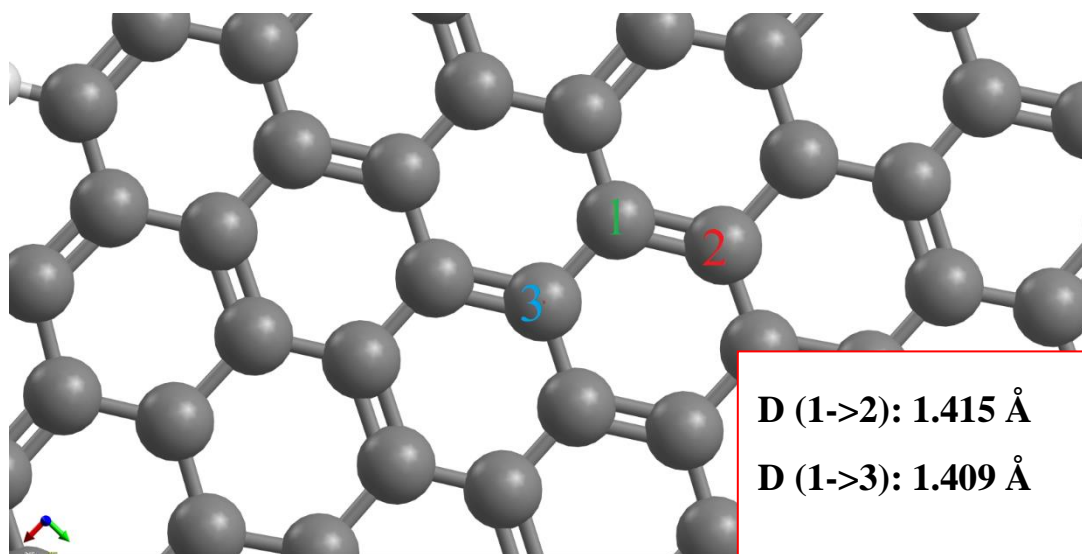**D (1->2): 1.415 Å**
**D (1->3): 1.409 Å**

Figure 6. Inset of image of bond lengths of C112 sheet.

On average, the calculation of C112 took just over 48 hours to converge with no added defects. When adding the Pd clusters to the sheet, we saw convergence time increase with increasing cluster size. This led us to believe that the C112 sheet would be the best option for use in our methodology that produced the most accurate results while keeping with reasonable computational effort.

## 4.2 Defective Graphene Optimization

The methodology presented here was to model how Pd clusters bonded to the graphene sheet explained in section 4.1. As keeping with current trends in applied catalysis, we have shown these Pd clusters bonding to the sheet in a created defect site[21,52]. This site was created by removing one, and two, carbon atoms respectively and bonding the cluster at that location. The optimized structures of defective graphene can be seen in Figure 7.

The carbon atoms when converged create a larger ring of carbon to compensate for the removal of one atom. While the single defect site is interesting in itself, it does not represent what is seen most commonly in defective graphene available on the market as a support for nanoparticles. Most defect sites are a few nanometers in length[53] which account for the removal of many carbon atoms and a sheet reconstruction. Although our study does examine both defect site and the effects on B.E. and I.E. of for the Pdn clusters we believe this model can point to how clusters of various sizes will interact with larger defective sites.
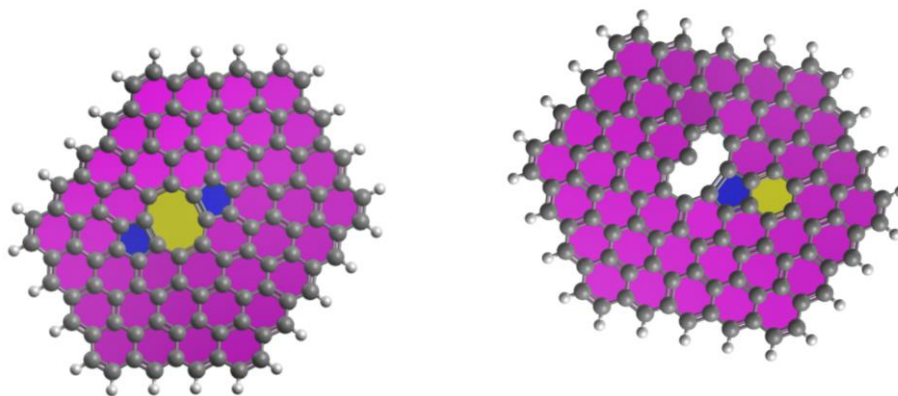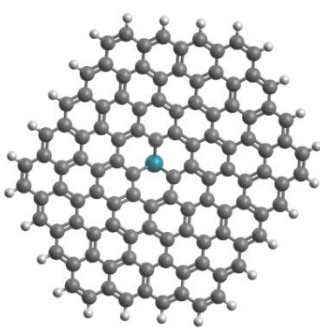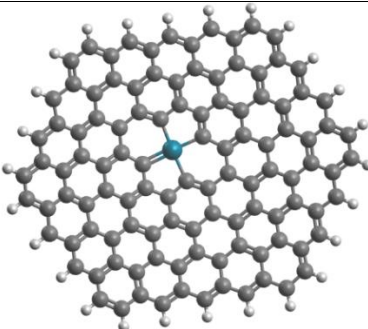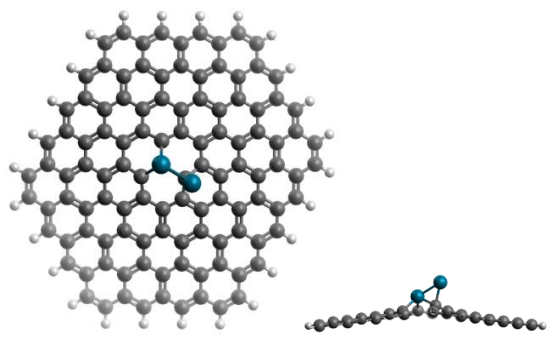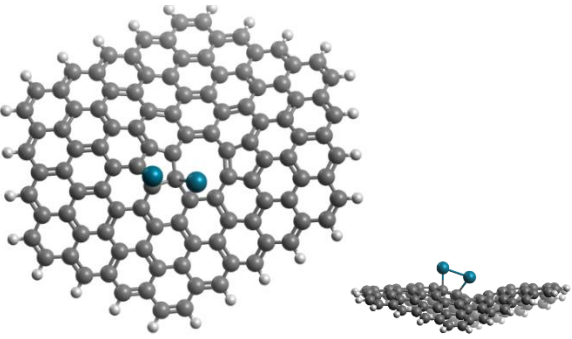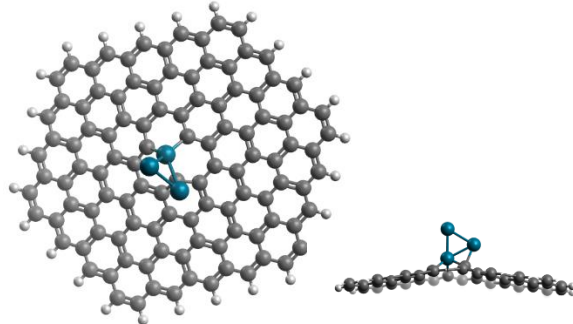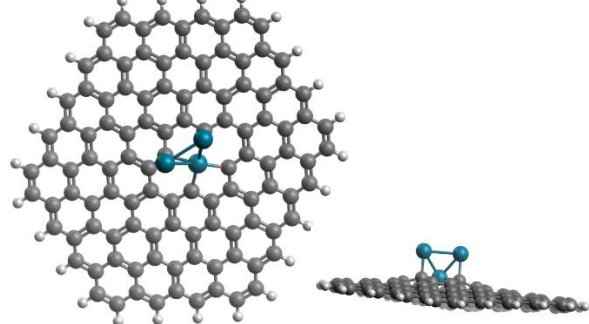


Figure 7. Images of optimized defective Pd Sheets of C112.

## 4.3 Pd Clusters on Defective Graphene

When Palladium clusters are bound to the graphene sheet results show that binding energy increases by an average of 3 eV from the ground-state energy calculations. These results would point to graphene being an excellent support for Pd nanoparticles because if the binding energy is stronger than an unbound particle it should increase the stability, and reduce sintering and agglomeration of the Pd particles.

| Cluster Structures on Graphene | | |
|---|---|---|
| Cluster Size | Single Defect | Double Defect |
| 1 |  |  |
| 2 |  |  |
| 3 |  |  |

| | | |
|---|---|---|
| 4 |  |  |
| 5 |  |  |
| 6 |  |  |
| 7 |  |  |

| 13 |  |  |
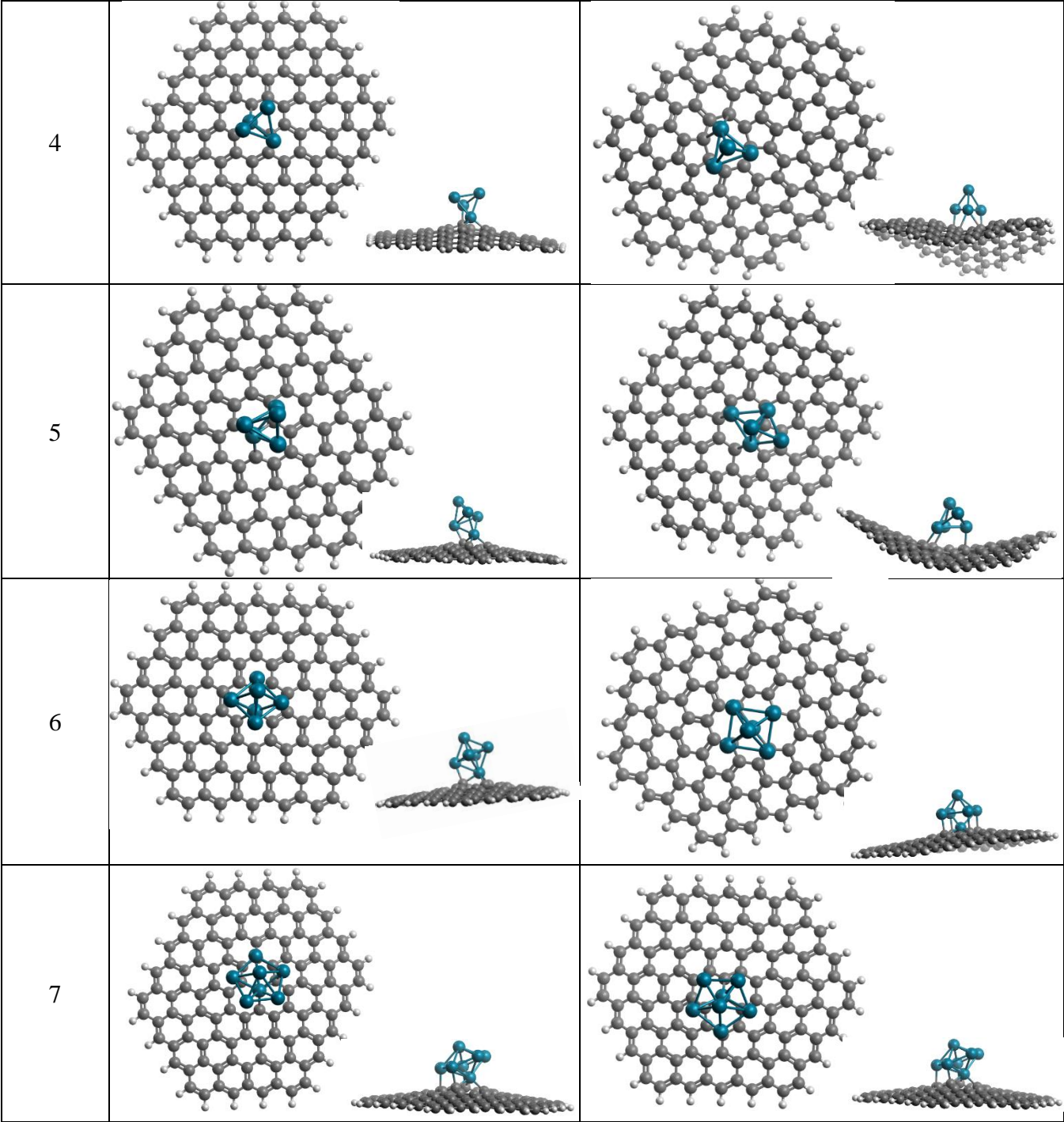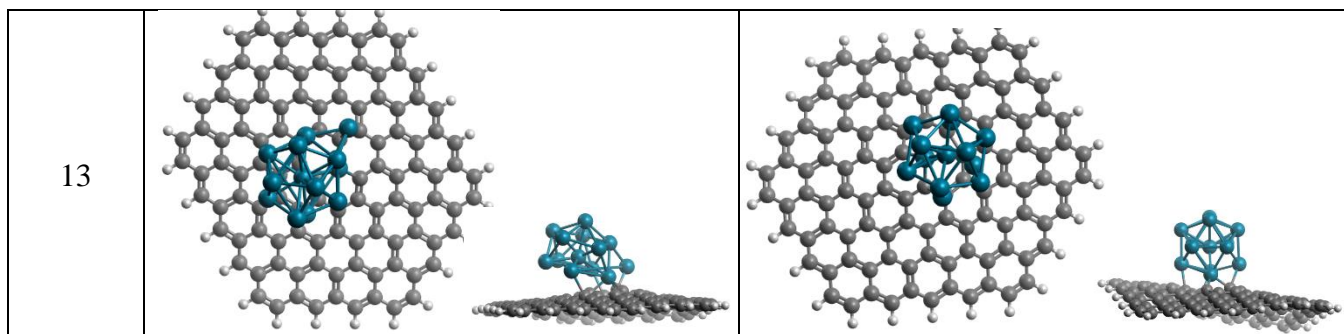
Table 4. Structures of Palladium Clusters on Defective Graphene

| Pd Cluster Effects on Defective Graphene | | | |
|---|---|---|---|
| | Ground-State Cluster | Single Defect Site | Double Defect Site |
| N | Coh. E. /atom (eV) | Pd Cohesive B.E. (eV) | Pd Cohesive B.E. (eV) |
| 1 | - | 4.846 | 2.302 |
| 2 | 0.543 | 3.487 | 2.197 |
| 3 | 1.097 | 3.041 | 2.413 |
| 4 | 1.502 | 2.907 | 1.809 |
| 5 | 1.615 | 2.815 | 2.200 |
| 6 | 1.747 | 2.510 | 2.519 |
| 7 | 1.877 | 2.790 | 3.852 |
| 13 | 2.087 | 2.735 | 2.459 |

Table 5. Binding Energies and ionization energies for clusters on defective graphene.

As seen in Table 4. The binding energy of Pd clusters on the single defect site decrease with increasing cluster size, similarly to the ground-state energy. The single Pd atom shows the largest binding energy of the bound species due to its direct replacement in the graphene lattice shown in Figure 8. Although the Pd atom is larger than a carbon atom by 0.067 nm it fits into the lattice by increasing the bond length on the sides around it also seen in Figure 8.
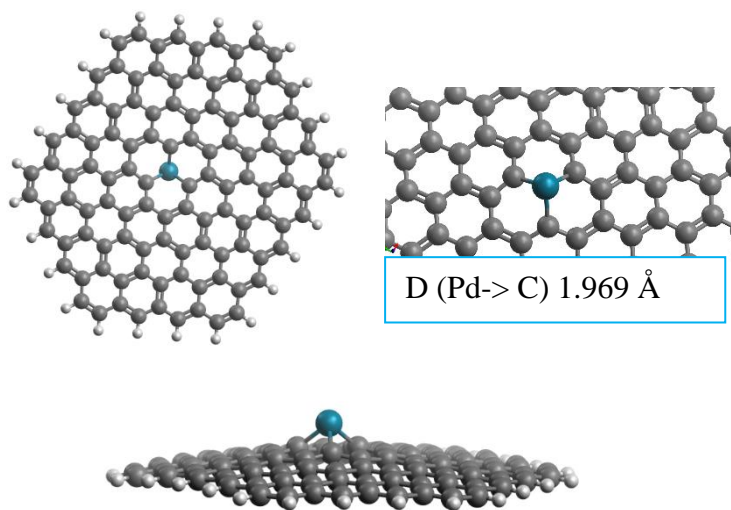


Figure 8. Pd atom on single defect site graphene.

As our clusters get larger, the geometry of the clusters begin to breakdown as they bind to the graphene sheet. In numerous cases, Pd3, and Pd4, one of the lower Pd atoms binds into the sheet similarly to the Pd atom while the other atoms remain unbound on top if that Pd atom. The cluster essentially is anchored by the bottom Pd atom into the defect site. However, this is not always true. With Pd7 the bottom atom is indeed anchored, but the outer "ring" of atoms is also bound to the sheet, seen as the increase in binding energy between Pd6 and Pd7 for the single defect.

The double defect does not show as nice of a trend as the single defect although it does have some of the same geometrical characteristics. Most of the bottom Pd atoms anchor further into the sheet and in the case of the single atom, it is bound by one double bond and 3 single bonds on

Figure 9. Pd atom on single defect site graphene.

each side. It seems as though this would create a stronger binding energy than compared to the

single defect site but that is not what our model shows. This could potentially be due to the increase in the size of the defect site where the Pd atom is not as closely bonded to each of the anchoring carbon atoms. In this instance, the bond length between the Pd atom and the three single bound C atoms is more than 2.0 Å and is easier to break than the tighter bonds in the single defect.

As clusters grown on the double defect a "cage" bonding effect begins to occur. The geometrically lowest atoms in the cluster bonds within the sheet and those in the plane above the sheet bind as well. This is clearly displayed in Figure 9. with the Pd5 cluster. Although this effect is seen in the converged structure, the binding energies do not seem to support that this makes the clusters bond more strongly to the sheet. In fact, it seems that the opposite is true because the binding energies in the double defect are less than the single defect but larger than the ground-state clusters.
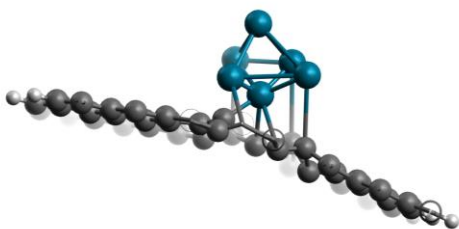


Figure9. Pd6 with "cage effect" bonds surrounding.

**Ionization Effects**

As a part of the study we sought to understand the effect of ionization on each of the clusters when bound to the defective graphene. Table 5. shows results of the +1 state on all Pd clusters. As seen the ionization energy has decreased from the unbound clusters. This decrease in I.E. would be favorable for many catalytic processes that rely on Pd particles being ionized within the cycle. Previous research has shown that graphene promotes the exchange of electrons throughout the surface[2,16]. Our study further back-up this thought with the evidence of the energy needed to remove and electron being easier when the Pd is bound than the free cluster. Geometrically the structures of the ionized clusters on the graphene sheets do not change a notable amount from the neutral clusters.

| Clusters on Graphene Ionization Energies (eV) +1 | | | |
| --- | --- | --- | --- |
| | Unbound Cluster | Single Defect Site | Double Defect Site |
| $N$ | I.E. | I.E. | I.E. |
| 1 | 8.973 | 5.191 | 5.408 |
| 2 | 7.642 | 5.210 | 5.262 |
| 3 | 7.734 | 5.194 | 5.272 |
| 4 | 6.810 | 5.186 | 3.930 |
| 5 | 6.654 | 5.155 | 5.293 |
| 6 | 6.419 | 3.241 | 5.273 |
| 7 | 6.358 | 5.208 | 5.342 |
| 13 | 6.323 | 5.466 | 5.329 |

Table 6. Ionization energies of clusters on defective graphene.

One remarkable result from this study is that the Pd4 on a double defect is found to have an extremely low ionization energy of 3.93 eV, putting it in the range of ionization energies for an alkali metal. As seen in Figure 10. The ionization energies decrease as the cluster is placed onto the defective graphene. In previous studies, $Pd_4$ on a double defect was found to a particularly good cluster for the Suzuki cross-coupling reaction.[22] This result seems to suggest that this particular size is an unusually good electron donor, meaning that it would be a better catalyst than other sizes. Pd6 on a single defect is also seen to have an usually low ionization energy, suggesting that this might also be an unusually good cluster for cross-coupling and other reactions that require the catalyst to act as a charge donor. In general, the defective support lowers the ionization energy from 1-2 eV, supporting our hypothesis that the graphene acts as a charge donating ligand that lowers the ionization of the cluster, and makes the cluster a more effective charge donor.
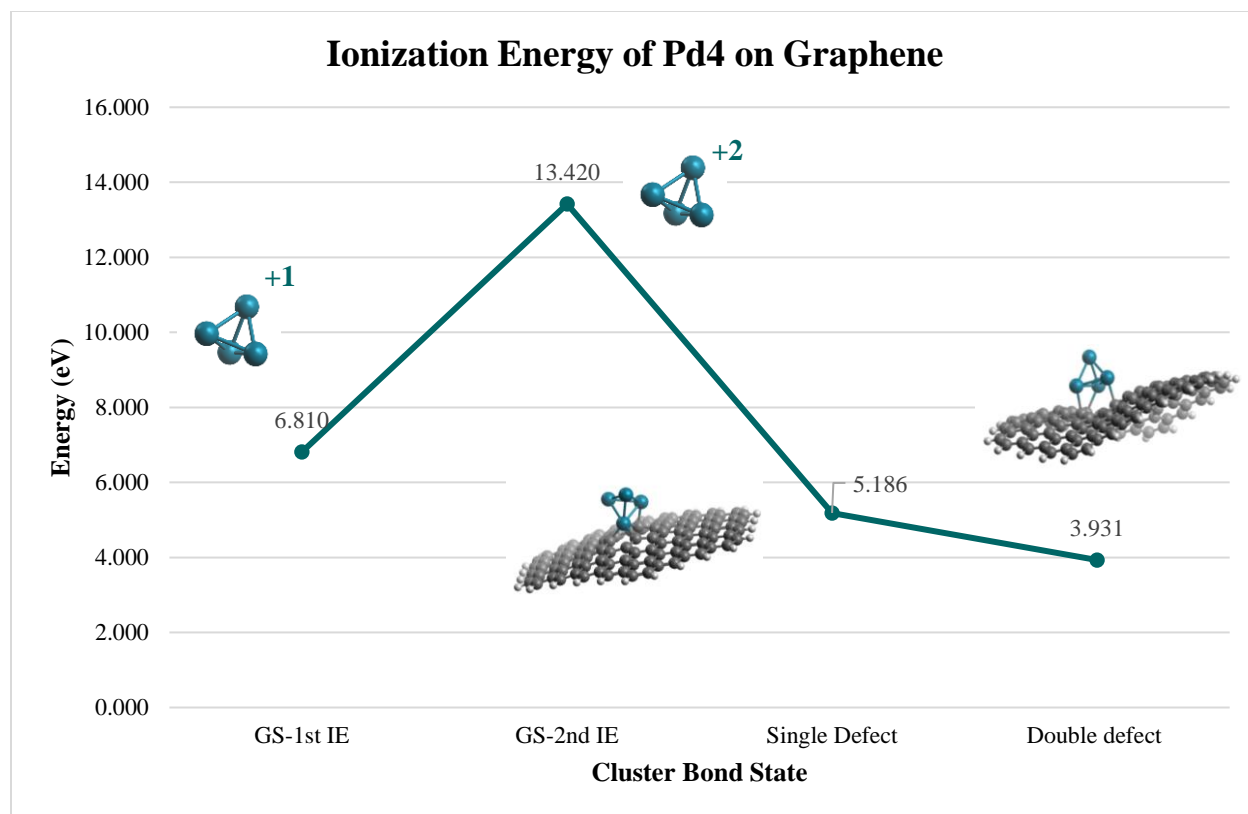
**Ionization Energy of Pd4 on Graphene**

Figure 10. Graph of Ionization Energy change as $Pd_4$ cluster is placed onto graphene support.

# Chapter 5. Conclusions

In this work we sought to investigate fully the effects that graphene has on Pd nanoparticles or clusters of a few atoms. When unbound, the DFT calculations performed found that clusters exhibit characteristics of binding energy and ionization energy that are in agreement with previous studies. As cluster size increases, binding energy increases due to increased bonding between the atoms. We found that when bound to a defective graphene sheet, ionization energy decreases as compared to the free cluster state, and decreases with increasing cluster size. This helps to explain why graphene activates the supported cluster, as the cluster becomes a significantly better charge donor when it is embedded in graphene. The graphene support acts as a charge donor that allows for the transfer of the charge through the sheet[16] and onto the cluster itself which would allow the particles to reach a charged state more easily than an unbound cluster or nanoparticle. This improved charge donation is crucial in the field of catalysis and our study provides further support that adding a substrate can alter the performance of small clusters of transition metal nanoparticles, and further

supports the hypothesis that the high activity of palladium particles supported on microwaved graphene is in part an electronic effect.

# Chapter 6. Future Directions

Options for further work on this topic are very wide reaching. Additional studies could be completed to elucidate information on how other transition metal species would interaction with a graphene support at similar cluster sizes. Specifically, Platinum, although more costly than Palladium, would be our first choice due to its similarity in both electronic structure and use in various applications. Interesting work could be performed regarding further charge states, specific binding sites on the graphene sheet, or adding functional groups to the graphene surface.

# Chapter 7. References

1. Bell, A. T. The Impact of Nanoscience on Heterogeneous Catalysis. *Science* **299**, 1688–1691 (2003).

2. Castro Neto, A. H., Guinea, F., Peres, N. M. R., Novoselov, K. S. & Geim, A. K. The electronic properties of graphene. *Rev. Mod. Phys.* **81**, 109–162 (2009).

3. Sanchez, A. *et al.* When Gold Is Not Noble:  Nanoscale Gold Catalysts. *J Phys Chem A* **103**, 9573–9578 (1999).

4. Roach, P. J., Woodward, W. H., Castleman, A. W., Reber, A. C. & Khanna, S. N. Complementary Active Sites Cause Size-Selective Reactivity of Aluminum Cluster Anions with Water. *Science* **323**, 492–495 (2009).

5. Kaden, W. E., Wu, T., Kunkel, W. A. & Anderson, S. L. Electronic Structure Controls Reactivity of Size-Selected Pd Clusters Adsorbed on TiO2 Surfaces. *Science* **326**, 826–829 (2009).

6. Kaden, W. E., Kunkel, W. A., Kane, M. D., Roberts, F. S. & Anderson, S. L. Size-Dependent Oxygen Activation Efficiency over Pdn/TiO2(110) for the CO Oxidation Reaction. *J Am Chem Soc* **132**, 13097–13099 (2010).

7. Luo, Z. *et al.* Spin Accommodation and Reactivity of Silver Clusters with Oxygen: The Enhanced Stability of Ag13–. *J. Am. Chem. Soc.* **134**, 18973–18978 (2012).

8. Kwon, G. *et al.* Size-Dependent Subnanometer Pd Cluster (Pd4, Pd6, and Pd17) Water Oxidation Electrocatalysis. *ACS Nano* **7**, 5808–5817 (2013).

9. Reber, A. C. & Khanna, S. N. Superatoms: Electronic and Geometric Effects on Reactivity. *Acc. Chem. Res.* **50**, 255–263 (2017).

10. Yang, Y., E Castano, C., Frank Gupton, B., C. Reber, A. & N. Khanna, S. A fundamental analysis of enhanced cross-coupling catalytic activity for palladium clusters on graphene supports. *Nanoscale* **8**, 19564–19572 (2016).

11. Moussa, S., Siamaki, A. R., Gupton, B. F. & El-Shall, M. S. Pd-Partially Reduced Graphene Oxide Catalysts (Pd/PRGO): Laser Synthesis of Pd Nanoparticles Supported on PRGO Nanosheets for Carbon–Carbon Cross Coupling Reactions. *ACS Catal.* **2**, 145–154 (2011).

12. Siamaki, A. R., Khder, A. E. R. S., Abdelsayed, V., El-Shall, M. S. & Gupton, B. F. Microwave-assisted synthesis of palladium nanoparticles supported on graphene: A highly active and recyclable catalyst for carbon–carbon cross-coupling reactions. *J. Catal.* **279**, 1–11 (2011).

13. Yang, X.-F. *et al.* Single-Atom Catalysts: A New Frontier in Heterogeneous Catalysis. *Acc. Chem. Res.* **46**, 1740–1748 (2013).

14. Jain, P. K., Huang, X., El-Sayed, I. H. & El-Sayed, M. A. Review of Some Interesting Surface Plasmon Resonance-enhanced Properties of Noble Metal Nanoparticles and Their Applications to Biosystems. *Plasmonics* **2**, 107–118 (2007).

15. Reber, A. C. & Khanna, S. N. Effect of N- and P-Type Doping on the Oxygen-Binding Energy and Oxygen Spillover of Supported Palladium Clusters. *J. Phys. Chem. C* **118**, 20306–20313 (2014).

16. Yang, Y. *et al.* More than just a support: Graphene as a solid-state ligand for palladium-catalyzed cross-coupling reactions. *J. Catal.* **360**, 20–26 (2018).

17. Keith, J. & Henry, P. The Mechanism of the Wacker Reaction: A Tale of Two Hydroxypalladations. *Angew. Chem. Int. Ed.* **48**, 9038–9049 (2009).

18. Bhaduri, S. & Mukesh, D. *Homogeneous Catalysis: Mechanisms and Industrial Applications*. (John Wiley & Sons, 2014).

19. Baeckvall, J. E., Akermark, B. & Ljunggren, S. O. Stereochemistry and mechanism for the palladium(II)-catalyzed oxidation of ethene in water (the Wacker process). *J. Am. Chem. Soc.* **101**, 2411–2416 (1979).

20. Marion, N. *et al.* Modified (NHC)Pd(allyl)Cl (NHC = *N* -Heterocyclic Carbene) Complexes for Room-Temperature Suzuki−Miyaura and Buchwald−Hartwig Reactions. *J. Am. Chem. Soc.* **128**, 4101–4111 (2006).

21. Li, Y. *et al.* Palladium nanoparticle-graphene hybrids as active catalysts for the Suzuki reaction. *Nano Res.* **3**, 429–437 (2010).

22. Yang, Y. *et al.* Donor/Acceptor Concepts for Developing Efficient Suzuki Cross-Coupling Catalysts Using Graphene-Supported Ni, Cu, Fe, Pd, and Bimetallic Pd/Ni Clusters. *J. Phys. Chem. C* **122**, 25396–25403 (2018).

23. Chauhan, V., Reber, A. C. & Khanna, S. N. Strong lowering of ionization energy of metallic clusters by organic ligands without changing shell filling. *Nat. Commun.* **9**, 1–7 (2018).

24. Chauhan, V., Reber, A. C. & Khanna, S. N. Transforming Ni9Te6 from Electron Donor to Acceptor via Ligand Exchange. *J. Phys. Chem. A* **120**, 6644–6649 (2016).

25. Reber, A. C., Bista, D., Chauhan, V. & Khanna, S. N. Transforming Redox Properties of Clusters Using Phosphine Ligands. *J. Phys. Chem. C* **123**, 8983–8989 (2019).

26. Reber, A. C., Chauhan, V., Bista, D. & Khanna, S. N. Superatomic molecules with internal electric fields for light harvesting. *Nanoscale* **12**, 4736–4742 (2020).

27. Reber, A. C. & Khanna, S. N. Co 6 Se 8 (PEt 3 ) 6 superatoms as tunable chemical dopants for two-dimensional semiconductors. *Npj Comput. Mater.* **4**, 33 (2018).

28. Bista, D., Chauhan, V., Sengupta, T., Reber, A. C. & Khanna, S. N. A ligand-induced homojunction between aluminum-based superatomic clusters. *Nanoscale* **12**, 12046–12056 (2020).

29. Metiu, H., Chrétien, S., Hu, Z., Li, B. & Sun, X. Chemistry of Lewis Acid–Base Pairs on Oxide Surfaces. *J. Phys. Chem. C* **116**, 10439–10450 (2012).

30. Reber, A. C. & Khanna, S. N. Effect of Embedding Platinum Clusters in Alumina on Sintering, Coking, and Activity. *J. Phys. Chem. C* **121**, 21527–21534 (2017).

31. Velde, G. te *et al.* Chemistry with ADF. *J. Comput. Chem.* **22**, 931–967 (2001).

32. van Lenthe, E., Snijders, J. G. & Baerends, E. J. The zero-order regular approximation for relativistic effects: The effect of spin–orbit coupling in closed shell molecules. *J. Chem. Phys.* **105**, 6505–6516 (1996).

33. Burke, K. Perspective on density functional theory. *J. Chem. Phys.* **136**, 150901 (2012).

34. Becke, A. D. Perspective: Fifty years of density-functional theory in chemical physics. *J. Chem. Phys.* **140**, 18A301 (2014).

35. Reed, B. C. *[Quantum Mechanics]*. (Jones and Bartlett Publishers, Inc, 2007).

36. Parr, R. G. Density Functional Theory of Atoms and Molecules. in *Horizons of Quantum Chemistry* (eds. Fukui, K. & Pullman, B.) 5–15 (Springer Netherlands, 1980). doi:10.1007/978-94-009-9027-2_2.

37. Simon, S. H. *The Oxford Solid State Basics*. (Oxford University Press, Usa, 2013).

38. Kohn, W. & Sham, L. J. Self-Consistent Equations Including Exchange and Correlation Effects. *Phys. Rev.* **140**, A1133–A1138 (1965).

39. Burke, K., Werschnik, J. & Gross, E. K. U. Time-dependent density functional theory: Past, present, and future. *J. Chem. Phys.* **123**, 062206 (2005).

40. Bagayoko, D. Understanding density functional theory (DFT) and completing it in practice. *AIP Adv.* **4**, 127104 (2014).

41. Perdew, J. P., Burke, K. & Ernzerhof, M. Generalized Gradient Approximation Made Simple. *Phys. Rev. Lett.* **77**, 3865–3868 (1996).

42. Cohen, A. J., Mori-Sánchez, P. & Yang, W. Insights into Current Limitations of Density Functional Theory. *Science* **321**, 792–794 (2008).

43. Moseler, M., Häkkinen, H. & Landman, U. Supported Magnetic Nanoclusters: Soft Landing of Pd Clusters on a MgO Surface. *Phys. Rev. Lett.* **89**, 176103 (2002).

44. Yudanov, I. V., Genest, A. & Rösch, N. DFT Studies of Palladium Model Catalysts: Structure and Size Effects. *J. Clust. Sci.* **22**, 433–448 (2011).

45. DFT Study of Small Palladium Clusters Pdn and Their Interaction with a CO Ligand (n = 1–9) - Zanti - 2009 - European Journal of Inorganic Chemistry - Wiley Online Library.

https://onlinelibrary-wiley-

com.proxy.library.vcu.edu/doi/full/10.1002/ejic.200900513?casa_token=EmCwSGcOAlkA

AAAA%3AdLd2d0j197LEZ2P4iM4hgXjaMT7fy2pD1AQEmkGumPR9x1fte4yAJbJ_eAFv

nkwveZXe1kZA2a4vClnE.

46. Nava, P., Sierka, M. & Ahlrichs, R. Density functional study of palladium clusters. *Phys*

*Chem Chem Phys* **5**, 3372–3381 (2003).

47. Chauhan, V., Reber, A. C. & Khanna, S. N. Strong lowering of ionization energy of metallic

clusters by organic ligands without changing shell filling. *Nat. Commun.* **9**, 2357 (2018).

48. Köster, A. M. *et al.* On the Ground State of Pd13. *J Am Chem Soc* **133**, 12192–12196 (2011).

49. Rezaei, M., Tabaian, S. H. & Haghshenas, D. F. Nucleation and growth of Pd nanoparticles

during electrocrystallization on pencil graphite. *Electrochimica Acta* **59**, 360–366 (2012).

50. Li, D. & Kaner, R. B. Graphene-Based Materials. *Science* **320**, 1170–1171 (2008).

51. Kane, C. L. & Mele, E. J. Quantum Spin Hall Effect in Graphene. *Phys. Rev. Lett.* **95**,

(2005).

52. Sun, T. *et al.* Facile and Green Synthesis of Palladium Nanoparticles-Graphene-Carbon

Nanotube Material with High Catalytic Activity. *Sci. Rep.* **3**, 2527 (2013).

53. Sen, D., Thapa, R. & Chattopadhyay, K. K. Small Pd cluster adsorbed double vacancy defect

graphene sheet for hydrogen storage: A first-principles study. *Int. J. Hydrog. Energy* **38**,

3041–3049 (2013).